Dual modality intravascular optical coherence tomography (OCT) and near-infrared fluorescence (NIRF) imaging: a fully automated algorithm for the distance-calibration of NIRF signal intensity for quantitative molecular imaging

Citation: Ughi, Giovanni J., Johan Verjans, Ali M. Fard, Hao Wang, Eric Osborn, Tetsuya Hara, Adam Mauskapf, Farouc A. Jaffer, and Guillermo J. Tearney. "Dual Modality Intravascular Optical Coherence Tomography (OCT) and Near-Infrared Fluorescence (NIRF) Imaging: a Fully Automated Algorithm for the Distance-Calibration of NIRF Signal Intensity for Quantitative Molecular Imaging." Int J Cardiovasc Imaging 31, no. 2 (October 24, 2014): 259–268.

As Published: http://dx.doi.org/10.1007/s10554-014-0556-z

Publisher: Springer Netherlands

Persistent URL: http://hdl.handle.net/1721.1/105793

Version: Author's final manuscript: final author's manuscript post peer review, without publisher's formatting or copy editing

Int J Cardiovasc Imaging (2015) 31:259–268
DOI 10.1007/s10554-014-0556-z

ORIGINAL PAPER

Dual modality intravascular optical coherence tomography (OCT) and near-infrared fluorescence (NIRF) imaging: a fully automated algorithm for the distance-calibration of NIRF signal intensity for quantitative molecular imaging

Giovanni J. Ughi · Johan Verjans · Ali M. Fard · Hao Wang · Eric Osborn · Tetsuya Hara · Adam Mauskapf · Farouc A. Jaffer · Guillermo J. Tearney

Received: 10 March 2014 / Accepted: 18 October 2014 / Published online: 24 October 2014

Abstract Intravascular optical coherence tomography (IVOCT) is a well-established method for the high-resolution investigation of atherosclerosis in vivo. Intravascular near-infrared fluorescence (NIRF) imaging is a novel technique for the assessment of molecular processes associated with coronary artery disease. Integration of NIRF and IVOCT technology in a single catheter provides the capability to simultaneously obtain co-localized anatomical and molecular information from the artery wall. Since NIRF signal intensity attenuates as a function of imaging catheter distance to the vessel wall, the generation of quantitative NIRF data requires an accurate measurement of the vessel wall in IVOCT images. Given that dual modality, intravascular OCT–NIRF systems acquire data at a very high frame-rate (>100 frames/s), a high number of images per pullback need to be analyzed, making manual processing of OCT–NIRF data extremely time consuming. To overcome this limitation, we developed an algorithm for the automatic distance-correction of dual-modality OCT–NIRF images. We validated this method by comparing automatic to manual segmentation results in 180 in vivo images from six New Zealand White rabbit atherosclerotic after indocyanine-green injection. A high Dice similarity coefficient was found (0.97 ± 0.03) together with an average individual A-line error of 22 μm (i.e., approximately twice the axial resolution of IVOCT) and a processing time of 44 ms per image. In a similar manner, the algorithm was validated using 120 IVOCT clinical images from eight different in vivo pullbacks in human coronary arteries. The results suggest that the proposed algorithm enables fully automatic visualization of dual modality OCT–NIRF pullbacks, and provides an accurate and efficient calibration of NIRF data for quantification of the molecular agent in the atherosclerotic vessel wall.

Keywords Optical coherence tomography · Optical frequency-domain imaging · Near-infrared fluorescence ·

Giovanni J. Ughi and Johan Verjans share first authorship.

Farouc A. Jaffer and Guillermo J. Tearney share senior authorship.

G. J. Ughi (✉) · A. M. Fard · H. Wang · F. A. Jaffer · G. J. Tearney
Wellman Center for Photomedicine, Harvard Medical School and Massachusetts General Hospital, Boston, MA, USA
e-mail: giovanni.ughi@mgh.harvard.edu

G. J. Tearney
e-mail: tearney@helix.mgh.harvard.edu

J. Verjans · E. Osborn · T. Hara · A. Mauskapf · F. A. Jaffer
Cardiovascular Research Center and Cardiology Division, Harvard Medical School and Massachusetts General Hospital, Boston, MA, USA

J. Verjans
Division of Heart and Lungs, Department of Cardiology, University Medical Center Utrecht, Utrecht, The Netherlands

H. Wang
Department of Biomedical Engineering, Boston University, Boston, MA, USA

E. Osborn
Cardiology Division, Beth Israel Deaconess Medical Center, Boston, MA, USA

G. J. Tearney
Department of Pathology, Harvard Medical School and Massachusetts General Hospital, Boston, MA, USA

G. J. Tearney
Harvard-Massachusetts Institute of Technology Health Sciences and Technology, Cambridge, MA, USA

Molecular imaging · Dual modality imaging · Cardiovascular imaging

Introduction

Atherosclerosis is the main cause of myocardial infarction, stroke and peripheral vascular disease. It is estimated that cardiovascular disease is the number one cause of death in the United States of America for both women and men >35 years old, with more than 700,000 deaths and 2 million cardiovascular procedures per year, half of them being catheterizations [1]. Direct and indirect costs of cardiovascular diseases have been estimated to be >300 billion dollars per year in the United States and are constantly increasing [1].

Intravascular optical coherence tomography (IVOCT) is a well-established method for the clinical investigation of coronary atherosclerosis [2]. It is an invasive catheter-based imaging modality using near-infrared light and interferometry, generating high-resolution images (i.e., axial resolution of ~10–15 μm) of coronary arteries and implanted devices [3]. Currently, IVOCT is extensively used for testing the safety and efficacy of novel treatments for atherosclerosis (e.g., drug-eluting stent and bioresorbable devices [4]) and for the guidance and optimization of complex percutaneous coronary interventions (PCI) [5].

Although IVOCT is capable of visualizing vessel wall microstructure and intraluminal objects (e.g., stent struts and intracoronary thrombus) in great detail [2], detection of molecular content and activity is not possible. Intravascular near-infrared fluorescence (NIRF) is an emerging molecular imaging modality aiming to improve the understanding of plaque and stent biology [6–9]. Therefore, simultaneous acquisition of NIRF data in conjunction with IVOCT would allow clinicians to gain insight regarding complementary molecular information in coronary disease [10]. More specifically, dual-modality intravascular OCT–NIRF allows for the first time the simultaneous acquisition of integrated information of vessel wall microstructure, composition and molecular processes (e.g. inflammation), making it suitable for multiple time-point assessment of novel treatments and better understanding of the natural history of atherosclerotic disease. For example, in the future, once available clinically, OCT–NIRF could allow one to identify areas of active inflammation in the context of other microstructural features (e.g., thin-cap fibroatheromas) assessing inflammation of high-risk vulnerable plaques in humans [7]. In addition, it could also enable a more precise characterization of molecular processes involved in neointimal tissue growth on stent surfaces [10, 11]. As such, this technology could prove very valuable in testing therapeutic efficacy of drugs (also on stents) to eventually prevent serious complications such as late stent thrombosis and stent neoatherosclerosis [12].

One of the current challenges for catheter-based dual-modality OCT–NIRF is that the fluorescence signal intensity decreases with the distance from the imaging catheter to the vessel wall, as the spot size decreases and the beam diverges. In order to generate quantitative NIRF data, the vessel wall position needs to be detected in IVOCT images and the detected NIRF signal intensity adjusted accordingly. Only calibrated NIRF data gives quantitative information about vessel wall fluorescence that represents the true concentration of NIRF molecular agents in the vessel wall. In a recent publication, the relationship between NIRF signal intensity and catheter-to-vessel wall was analyzed [10]. However, the data processing was done manually, and as a result, the process was very time consuming. Dual modality OCT–NIRF systems acquire images at a very high frame-rate and a high number of images per pullback need to be analyzed. As such, the manual analysis and calibration of NIRF data is impractical for large clinical studies and unsuitable for real-time intravascular OCT–NIRF image visualization. Therefore, an important step toward the clinical translation of dual-modality OCT–NIRF is the development of automated algorithms for rapid generation of quantitative NIRF data.

We have developed and validated a method for the fully automatic quantification of vessel wall position in IVOCT images and the subsequent calibration of NIRF data over an entire dual modality dataset in vivo in rabbit aortic vessels (which are of similar caliber as human coronary arteries) following intra-venous injection using indocyanine green (ICG) (IC-Green®, Akorn, Lake Forest, Illinois) a NIRF imaging agent targeting inflamed atherosclerotic plaques [7]. Similarly, validation was also obtained using clinical, coronary IVOCT data that was previously acquired. This algorithm may enhance translation of OCT–NIRF technology by facilitating the interpretation of OCT–NIRF datasets so that they can be readily acted upon in the cardiac catheterization lab.

Methodology

Experimental setup

The experimental system used in this study has been previously described [10]. We utilized a high-speed second-generation form of OCT termed optical frequency domain imaging (OFDI), also known as frequency domain OCT (FD-OCT) and swept source OCT (SS-OCT) [13, 14]. In brief, the OFDI and NIRF systems were developed independently and combined together by a dual modality rotary junction. Light separation for OFDI–NIRF imaging is

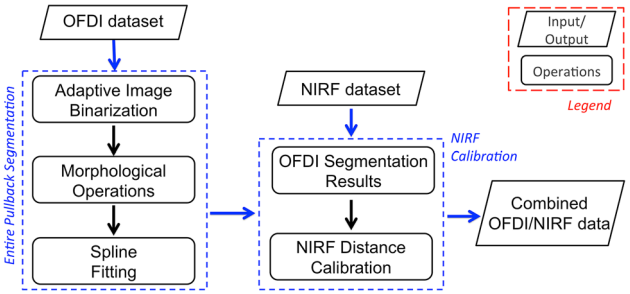

Fig. 1 Flowchart of the processing algorithm. The algorithm receives the entire IVOCT pullback and the co-registered NIRF dataset as inputs, automatically processes the data, and outputs the distance-calibrated IVOCT–NIRF pullback. No user interaction is required at any of the processing steps

obtained through the use of specific dichroic mirrors designed to split OFDI light wavelength (1,320 ± 55 nm) from NIRF light wavelength (750 nm). The imaging catheter is made of a double-clad fiber (DCF) (FUD-3236, Nufern, East Granby, CT), where the OFDI signal propagates through the fiber core (diameter of 9.7 μm) and the NIRF signal through the fiber cladding (diameter of 125 μm). The light is focused to the sample and subsequently detected by a ball lens (diameter of 320 μm) optimized for OFDI–NIRF dual modality imaging. Such a lens is produced through a dedicated procedure by splicing a short segment of coreless fiber on the tip of the DCF, which is subsequently shaped to a ball using a computer controlled laser splicing workstation (LZM-100 Laser Splicing System, AFL, Duncan, SC). The resulting ball lens is subsequently polished to a predefined angle (i.e., 38°) for side-view imaging. The fiber is then inserted into a metallic drive shaft (Terumo Corporation, Tokyo, Japan) with a housing specifically designed for accommodating the ball-lens on its tip. To protect the vessels during rotation and retraction of the drive shaft (i.e., data are acquired through a helical scan), the drive shaft is finally inserted in a transparent plastic sheath with an outer diameter of 800 μm (Terumo Corporation). This dual modality imaging system acquires OFDI images with an axial resolution of ~10–15 μm and a lateral resolution of ~30–60 μm. The A-scan line acquisition of OFDI and NIRF signal are synchronized at a speed of 52 kHz, so that the system simultaneously acquires co-localized OFDI–NIRF data.

Algorithm for OFDI–NIRF data processing

A flowchart of the processing algorithm is illustrated in Fig. 1. The algorithm receives two inputs: the entire IVOCT pullback and the co-registered NIRF dataset. The data processing workflow can be divided in two steps: (1) the vessel wall is automatically segmented through all IVOCT images at once; (2) quantitative information about the vessel wall position is then applied for the distance calibration of NIRF data. It is important to underline that this procedure runs in a fully automatic way and no user interaction is required.

Automatic segmentation

The aim of the segmentation is to provide an automatic, robust and time efficient quantification of the vessel wall position in intravascular IVOCT images. For this purpose, we propose a three-dimensional (3D) segmentation algorithm capable of analyzing an entire IVOCT dataset at once. Given that IVOCT images are collected through a helical scan (i.e., individual A-scan lines are acquired while rotating and retracting the imaging catheter), it is possible to represent an entire IVOCT pullback through a single image I_{pull} obtained concatenating individual polar domain images next to each other, as illustrated in Fig. 2. In this way, it is possible to analyze the entire pullback at the same time (i.e., not analyzing images one by one), taking advantage of the spatial continuity of the vessel. In addition, by looking at Fig. 2, one can argue that in IVOCT data there is more information than just an intensity increase between the lumen-vessel wall boundaries for differentiating between these two regions. The lumen is visualized as a low-intensity and non-textured region (with artifacts and intraluminal objects responsible for high intensity), while the vessel wall is a high-intensity textured region. A robust segmentation of the vessel wall can thus be achieved exploiting these properties.

As a first step, an adaptive binarization procedure is applied. Data are made binary by applying Otsu's method to I_{pull}, minimizing the variance between the two classes composing the image and thus providing a good separation for image foreground and background [15], which are in this case the vessel wall and the vessel lumen, respectively. However, vessel wall grayscale intensities acquired by IVOCT are dependent on the catheter position in the lumen (i.e., distance and angle of incidence of light), resulting in a variation of the image illumination along the pullback direction. As such, Otsu's method is applied to I_{pull} by the mean of a translating window w_s without overlap (as illustrated in Fig. 3a), resulting in an adaptive binarization of IVOCT data. Subsequently, the binary image I_{BW} (Fig. 3b) is processed with the purpose of retaining the vessel wall only. The vessel wall typically appears as a thick object with a regular and continuous profile, while the vessel lumen appears as a low intensity region and intraluminal objects (e.g., blood residuals and guide-wire) as irregular and isolated structures with a smaller area (e.g., Fig. 3a, yellow arrow). Appropriate morphological operations can be applied to the binary image for discriminating the vessel wall from other intraluminal objects. First, an

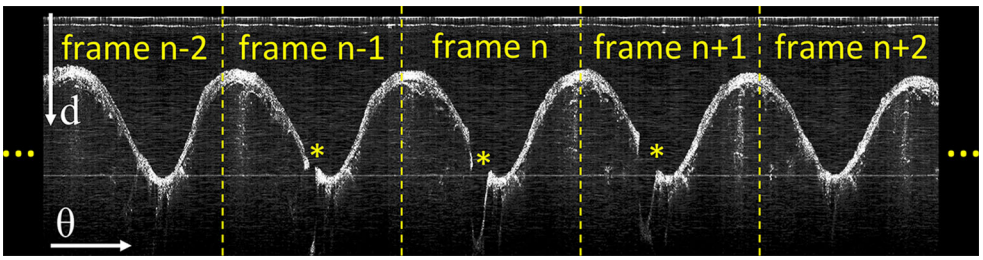

Fig. 2 IVOCT data are generated by acquiring a high number of A-scan lines per second while rotating and retracting the imaging catheter (i.e., helical acquisition). As such, an IVOCT pullback can be represented by a single image I_{pull} obtained by concatenating all the polar domain images (where data are represented as depth d vs. the acquisition angle θ) next to each other. The *yellow asterisk* indicates a side-branch and the *dotted lines* separation between different pullback frames

Fig. 3 Lumen-vessel wall segmentation procedure. **a** Part of the entire image I_{pull} representing the IVOCT pullback. *Yellow arrows* indicate blood residuals and the asterisks a side-branch and w_s is the translating window used for binarization. **b** Binarization results I_{BW} and **c** is the binary image I_{seg} after morphological processing. **d** Lumen-vessel wall segmentation results after spline fitting $f(p)$ for spatial continuity. A small offset has been applied to the location of lumen contour so that is displayed slightly inside the vessel lumen, to enhance its visualization

image closing operation is applied to I_{BW} using a disk-structuring element d_{se}, with the purpose of consolidating the vessel wall filling small holes in the binary image (Fig. 3c). Such image closing operation can defined as:

$$I_{closed} = I_{BW} \cdot d_{se} = (I_{BW} \oplus d_{se}) \ominus d_{se},$$

where $\oplus$ and $\ominus$ denotes dilation and erosion, respectively [16]. Subsequently, an area opening procedure eliminating all the 4-connected components with an area smaller than a predefined threshold T_{area} (e.g., blood residuals and guide-wire) is applied to I_{closed} obtaining the final binary image I_{seg} (Fig. 3c). To conclude this procedure, a cubic smoothing spline $f(p)$ [17] is fitted through the external profile of I_{seg}, generating the final segmentation contour (p indicates the smoothing parameter of the spline). Importantly, the use of a spline takes into account the spatial continuity of the vessel, corrects for eventual irregularities, and interpolates missing luminal contours in

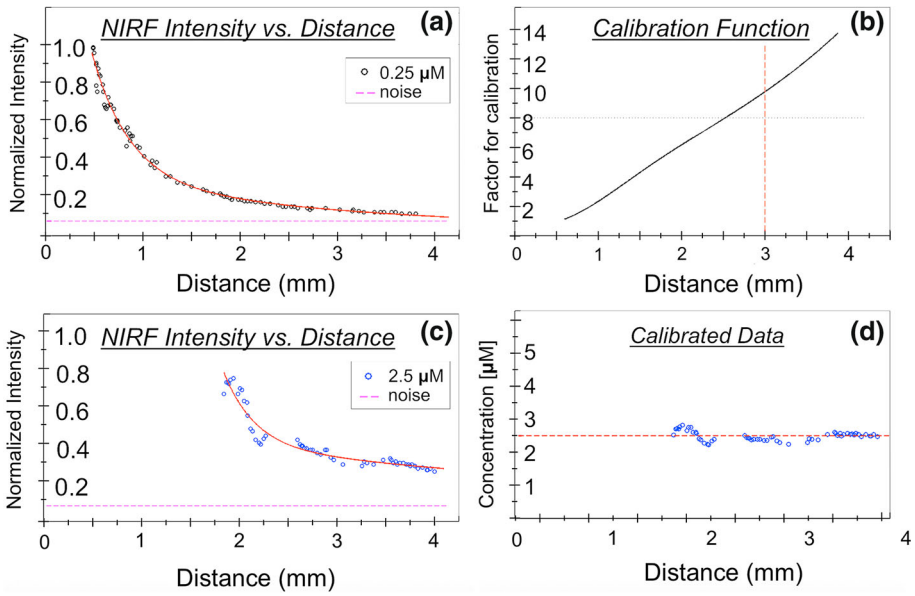

Fig. 4 **a** NIRF data for the 0.25 μM phantom and the exponential fitting $f(x)$ through the data (*red line*). **b** NIRF calibration function $g(x)$ estimated as $1/f(x)$. **c** and **d** NIRF data collected from the 2.5 μM phantom and the distance-calibration results obtained applying the calibration function g(x), respectively

the case of discontinuities, as illustrated in Fig. 3d. As such, this approach is also able to handle the presence of side-branches: if no tissue from the side-branch is visible then the branch is automatically excluded, otherwise the side-branch is part of the automatically traced contour. The final output of this segmentation algorithm is the position of the vessel wall for each A-line of the analyzed pullback.

NIRF signal compensation for quantitative NIRF imaging

Once the distance between the catheter and the artery wall was automatically determined, distance correction was applied in a similar way to what was previously described [10]. Briefly, to characterize the relationship between the detected NIRF signal intensity and vessel wall-catheter distance for the specific catheter used in this study, we prepared two phantoms using capillary tubes (with an inner and outer diameter of 0.8 and 1.2 mm, respectively) by filling them using saline solutions with different concentrations of a fluorescent dye (i.e., indocyanine green) of 2.5 and 0.25 μM, respectively. Phantoms were imaged by the OCT–NIRF experimental system in a plastic box filled with saline, acquiring images at different distances between the catheter and the phantom by the means of a pullback. Figure 4a shows NIRF data for the 0.25 μM phantom, plotting the NIRF signal intensity as a function of the distance from the imaging catheter that is defined using co-registered IVOCT images. Measurements were fitted using an exponential model $f(x) = a*exp(b*x) + c*exp(d*x)$ (a sum of exponential was selected as it provided a smaller fitting error compared to other models such as single exponential and logarithmic), and a calibration function for NIRF data was then obtained as $g(x) = 1/f(x)$ (Fig. 4b). With the purpose of validating such a function, NIRF signal intensity acquired from the second phantom (i.e., 2.5 μM concentration, Fig. 4c) was distance-calibrated using $g(x)$ (Fig. 4d). The two concentrations of 0.25 and 2.5 μM were selected so that there was a significant difference (i.e., one order of magnitude) between the two phantoms for generating and validating $g(x)$. The accuracy of $g(x)$ was subsequently estimated as the average variation, expressed in percentage, of calibrated data from the expected value of 2.5 μM. Such an estimated function $g(x)$, in combination with IVOCT segmentation results, enabled for the automatic calibration of NIRF signal intensity through all the individual A-scan lines comprising a dual-modality OCT–NIRF pullback.

Implementation details

Segmentation, scan-conversion and NIRF compensation algorithm were implemented in Matlab 2013a (MathWorks, Natick, MA) and additional toolboxes (i.e., Curve Fitting toolbox ver. 3.3, Image Processing toolbox ver. 8.1 and Statistics toolbox ver. 8.1). The algorithm processing time was quantified on a desktop computer (late 2010 iMac, Apple, Cupertino, CA), utilizing an i7 quad-core processor (Intel, Santa Clara, CA) and 12 Gb of RAM, in total.

Parameter tuning

The proposed segmentation algorithm was specifically designed to limit the number of parameters that needs to be tuned, which may decrease the sensitivity of the algorithm to the make/model of the IVOCT system, and should make the procedure easy to adapt for data acquired with different

IVOCT systems and settings. As such, a total of only four parameters needed to be tuned. Parameters were empirically defined by the means of a training-set (used for manual optimization) comprised of multiple OCT–NIRF images from n = 2 in vivo datasets.

In detail, the width of the sliding windows w_s was set equal to 128 A-scan lines. A high value for this parameter would make the algorithm more robust to artifacts and suboptimal quality of images (e.g. incomplete blood-flush during acquisition) while a lower value may allow for a more detailed segmentation in case of optimal image quality. The value of 128 (i.e., splitting each IVOCT image in 8 different "quadrants" according to the acquisition angle θ) was empirically selected, providing a good tradeoff between algorithm robustness and accuracy. Moreover, to understand the algorithm's dependence on this important parameter, we assessed the effect of a variation of ±15 % of the length of w_s on the segmentation results.

The size of the structuring element d_{se} for morphological image dilation was set to be equal to 12 pixels and the area constrain threshold (i.e., for the removal of small isolated structures as detailed on "Automatic segmentation" section) was set equal to 5×10^3 pixels. Both of these parameters are related to polar IVOCT image size, which in this case was 1,024 × 1,024 pixels, with 1,024 being both the number of A-lines per image and the number of samples per A-line. Finally, the smoothing spline parameter p was set equal to 0.1 for the purpose of generating a smooth vessel wall contour.

Data acquisition

IVOCT pullbacks were acquired in vivo in an established animal model of atherosclerosis [6, 7, 10]. New Zealand White rabbits (n = 8) developed atherosclerotic lesions after balloon de-endothelialization injury followed by a high cholesterol diet. The mean weight of the rabbits was 3.87 kg. Imaging was performed at 8 weeks acquiring one pullback from eight different rabbit abdominal aortas. Two (2) of them were used to generate the dataset for optimization of parameters, while the remaining six were used for algorithm validation. Data were acquired at a pullback speed of 10 mm/s (resulting in a longitudinal sampling of 0.4 mm in the pullback direction), typically imaging vessel segments of approximately 60 mm in length. An imaging agent, indocyanine green (ICG) (IC-Green®–Akorn, Lake Forest, Il), was injected for fluorescence imaging at a concentration of 0.5 mg/kg. OCT–NIRF imaging was performed 45 min after injection (n = 8 animals) as previously indicated [6, 7]. Data were acquired using a dual modality OCT–NIRF catheter, specifically fabricated for this study. The same catheter was used for all in vivo imaging sessions and phantom experiments.

Validation

The algorithm was validated by comparing automatic results to the manual segmentation performed by an expert image reader, which is the current gold standard for IVOCT image analysis [2]. Each luminal contour was manually traced by following the boundaries between the vessel lumen and the vessel wall (using ImageJ [18] working at an image magnification level of 1.5×). All the six test-set pullbacks were analyzed by assessing images with a sampling rate of 2 mm along the pullback direction (in order to not use multiple frames with similar features in the validation set), including images of both optimal and suboptimal quality. Manual and automatic 2D segmentation results (i.e., segmentation of individual cross sectional images) were compared by the means of the Dice similarity coefficient, a standard technique for assessing 2D segmentation accuracy (i.e., quantifying the agreement between automatic segmentation with respect to the gold standard) [19]. Moreover, the segmentation error over individual A-scan lines (1D) was also quantified through the median value and the mean absolute deviation [20]. To conclude the validation procedure, the correlation between the two measurements was also quantified using the Pearson's correlation coefficient.

In addition, the segmentation algorithm was also validated on previously acquired IVOCT clinical data. A total of 120 randomly extracted images from 8 different patients (eight pullbacks from human coronary arteries) were automatically and manually analyzed as described above. Results were quantified in the same manner: Dice similarity coefficient, individual A-scan lines error and correlation coefficient.

Results

A total of 300 images were included in the validation study (n = 180 preclinical and n = 120 clinical). A Dice similarity coefficient of 0.97 ± 0.03 (mean and standard deviation) was found comparing automatic to manual IVOCT vessel wall segmentation for preclinical data. The same value of 0.97 was found by applying a variation of ±15 % to the parameter w_s. In addition, a segmentation error of 22.0 μm (median value) and 36.5 μm (mean absolute deviation) was found over individual A-scan lines, together with a very high correlation coefficient of 0.99. Validation on IVOCT clinical images showed a Dice similarity coefficient of 0.96 ± 0.03, a segmentation error

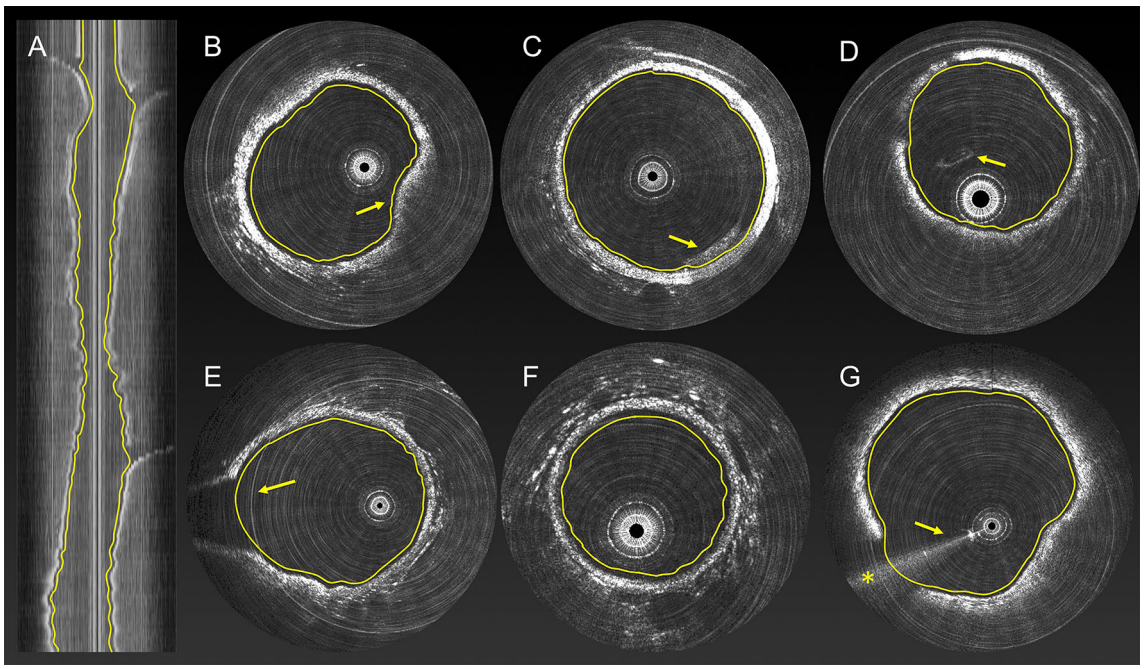

Fig. 5 Examples of fully automatic lumen-vessel wall segmentation for some specific cases. **a** Lateral reconstruction of an entire pullback with the segmentation displayed on the *top* (*yellow line*). **b** Case of irregular lumen contour due an atherosclerotic plaque (*yellow arrow*) and **c** and **d** show examples of residual blood in the vessel lumen (*yellow arrows*) and eccentric catheter position (**d**). The *yellow arrow* in (**e**) points to a side-branch. **f** An example of segmentation results in case of a small lumen diameter (~2 mm) and eccentric imaging catheter position. **g** An example of images where the guide-wire is present (*yellow arrows*). From this example, it can be seen that the algorithm is able to correctly handle the presence of the guide-wire even in case of "saturation artifact" (*yellow arrow*). The algorithm accurately spans the gap in the image where the wall is hidden by the guide-wire shadow (*yellow asterisk*). Similarly to Fig. 3, a small offset is applied to the lumen contour so that it is slightly inside the vessel lumen, in order to improve its visibility

of 26.4 ± 48.4 μm and a correlation coefficient of 0.99. Regarding NIRF calibration accuracy, the average variation of $g(x)$ from the expected value using the validation phantom with a concentration of 2.5 μM, was quantified to be equal to ~8 %. A computation time of approximately 44 ms per image was found, allowing to process an entire pullback of 200 images with 1024 A-scan lines per image in approximately 8.8 s.

Figure 5 shows examples of lumen segmentation for some specific situations. In panel (b) it is possible to observe a lipid plaque generating an irregular vessel wall profile. Panel (c) and (d) show examples of suboptimal image quality caused by residual blood in the vessel's lumen. Panel (e) shows a case with a side-branch, and in panel (g) segmentation results in the presence of a guide-wire saturation artifact. In all cases the segmentation algorithm correctly dealt with this particular confounding factors.

Discussion

In this study, we have described an algorithm for the automatic segmentation of intravascular IVOCT datasets and the subsequent calibration of NIRF signal intensity. The algorithm is fully automatic and was validated over a large number of images acquired in vivo (i.e., 180 images from 6 in vivo preclinical IVOCT–NIRF datasets and 120 images from 8 IVOCT in vivo pullbacks of human coronary arteries, including real-life cases of suboptimal image quality and artifacts. Validation results showed that the algorithm provides very accurate results and that an entire dataset can be processed in a rapid and efficient manner. Moreover, the validation study showed that parameters do not need to be retuned among different acquisitions, including both clinical and preclinical data, and that the algorithm can be easily be applied to different datasets acquired under different imaging conditions.

Given the fact that the manual segmentation of IVOCT images is extremely time consuming (e.g., 1 h or more per dataset, compared to the few seconds required by the automated algorithm), validation results suggest that the proposed algorithm can replace manual analysis achieving a more efficient processing that is suitable for the on-line visualization of dual modality OCT–NIRF pullbacks. This algorithm enables the automatic processing of these dual-modality images in a rapid and effective way, making it possible to visualize quantitative NIRF data immediately after OCT–NIRF pullback acquisition. As a matter of fact, the proposed method can potentially be integrated on

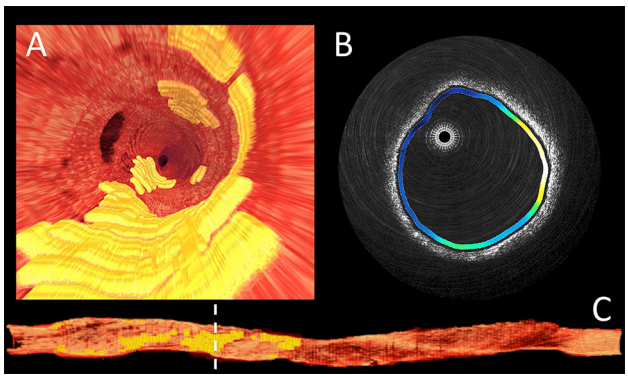

Fig. 6 3D rendering of the entire IVOCT–NIRF calibrated pullback (**a** and **c**). *Red color* represents the vessel wall and *yellow color* a high NIRF signal. **b** An example of combined intravascular OCT–NIRF cross-sectional image after NIRF signal calibration. The proposed method for the automatic processing of intravascular OCT–NIRF datasets can potentially facilitate the generation and display of combined 3D morphological and molecular information of the vessel at the time of the percutaneous coronary intervention. OCT–NIRF 3D rendering was obtained using software OsiriX (OsiriX Foundation, Geneva, Switzerland)

OCT–NIRF imaging systems, enabling automatic quantification of morphological, molecular and functional tissue information during percutaneous coronary intervention. In addition, the automated segmentation algorithm may enable the visualization an OCT–NIRF dataset in three-dimensions, providing an immediate representation of the entire vessel that is being visualized (Fig. 6). Furthermore, the proposed algorithm can potentially facilitate reliable and practical analysis of dual modality OCT–NIRF datasets in the context of core-lab analysis, where a large number of images typically need to be processed. Automatic lumen segmentation can also provide quantitative morphological information in an accurate and efficient manner, automatically identifying severity (i.e., minimal cross sectional area) and the extent of atherosclerotic lesions in IVOCT pullbacks. Manual processing does not allow for a quick visualization of quantitative OCT–NIRF data at the time of data acquisition and makes the generation of quantitative NIRF data cumbersome and inefficient. As such, the proposed method may be an important step for the clinical translation of dual modality intravascular OCT–NIRF imaging modality as a novel tool for the real-time assessment of human atherosclerosis, helping the optimization of current cardiovascular therapies and treatments.

Further improvements

The proposed algorithm was validated analyzing 300 images from 6 in vivo real-life intravascular OCT–NIRF datasets and 8 clinical IVOCT datasets obtained in vivo. Study results showed that the algorithm provided good quality segmentation without any systematic error with respect to manual analysis (gold standard available) without the need to re-tune the algorithm's parameters for different pullbacks. Validation in over 14 pullbacks obtained in vivo did not show confounding factors where the proposed method systematically fails. As such, we can conclude that in case of pullbacks with acceptable image quality (e.g., proper blood flushing of the vessel lumen during image acquisition), the proposed algorithm segments IVOCT accurately. If, in the future, additional improvements are necessary to increase accuracy, the algorithm can be furthered developed taking into account the "full" 3D spatial continuity of the vessel, as illustrated in Fig. 7. However, intravascular image acquisition artifacts such as non-uniform rotation distortion (NURD) and the relative movement of the imaging catheter with respect to the vessel wall may cause subsequent IVOCT images to not to be perfectly aligned with each other. Given that IVOCT is truly a high resolution imaging modality, even very small artifacts (e.g., tenths of microns) may play a significant role. Previous studies showed that these types of artifacts are very challenging to correct by applying post-processing methods only [21]. As such, future generations of IVOCT systems that can minimize these effects (e.g., using a motion tracking system [22] or through ultra-fast IVOCT image acquisition [23]), potentially enabling additional improvements in automated segmentation accuracy.

If compared to other (commercially) available methods [24, 25], the segmentation algorithm proposed in this paper contains similar features: the lumen contour is traced in a fully automated way, without the need of manual input from the user. However, if compared to previous methods [25], the key innovation introduced by this method is that an entire IVOCT pullback is segmented at once, processing the entire dataset as a single image. This methodology has the advantages of making this approach very efficient in terms of processing time (i.e., low complexity) and, as confirmed by the validation study, is very robust with respect to segmentation accuracy. However, a full comparison of this algorithm to other methods would require the use of a common datasets and the efforts from multiple groups involved in this research field, which is beyond the scope of this study.

Regarding suboptimal image quality, even the most accurate automated segmentation algorithm occasionally fails due unanticipated image features (e.g., artifacts) that are encountered in real world settings. Accordingly, a user interface is also under development to enable easy and efficient use of the software by intravascular OCT–NIRF operators in a catheterization lab. As typically done in the field of medical imaging, such an interface allows for a rapid inspection and manual correction of segmentation results in case of inaccuracies, making the algorithm

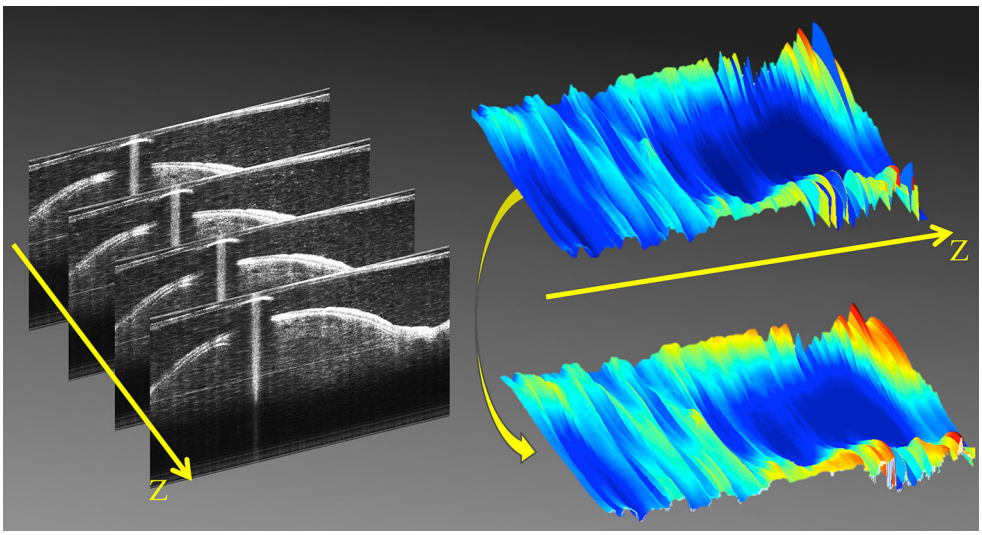

Fig. 7 *Left image* illustrates the 3D spatial continuity of IVOCT datasets along the pullback direction (polar image domain). The image on the *top right* represents the 3D pullback segmentation obtained by fitting a surface through individual segmented contour of adjacent images. Although the proposed algorithm gives excellent results only considering 2D spatial continuity through the IVOCT helical acquisition, 3D spatial continuity can also be taken into account smoothing irregularities on this 3D surface (*bottom right image*). However, in order to apply such a procedure, IVOCT images needs to be perfectly aligned to each other, which is often not the case for today's IVOCT systems. Future generation IVOCT systems, that minimize the effect of movement artifacts during data acquisition (e.g. ultrafast pullback acquisition or motion tracking systems), may allow an even more accurate 3D segmentation of intravascular IVOCT pullbacks

suitable for the analysis of data of very low quality or that contains rare artifacts.

As a last consideration, even using relatively computationally inefficient software (Matlab) and processor (Intel i7), the total time to process the IVOCT frame and correct the corresponding frame's NIRF signal was relatively good (44 ms). Optimization of the proposed algorithm using a graphic processing unit and implementation in a faster language (e.g., C++ or CUDA parallel processing) will accelerate the time to conduct automated image analysis further. Importantly, this optimization may enable for the display of quantitative NIRF data in real time. Near instantaneous display and registration of both IVOCT and quantitative NIRF data in the catheterization lab is an important step that will require to make this information actionable. This automated process will therefore become critical once studies have been conducted that show the clinical benefit of intravascular OCT–NIRF.

Acknowledgments NIH R01HL093717 (GJT—development of imaging system), R01HL108229 (FAJ), AHA Grant-in-Aid 13GRNT1760040 (FAJ), MGH SPARK Award, Bullock-Wellman Fellowship Award/Harvard Medical School and Massachusetts General Hospital (GJU), Harvard Catalyst NIH 1UL1 TR001102-01 (EO), Rubicon Grant 825.12.013/Netherlands Organization for Scientific Research (JV), and Merck (GJT and FAJ).

Conflict of interest Dr. Tearney receives catheter materials from Terumo Corporation. Massachusetts General Hospital has a licensing arrangement with Terumo Corporation. Dr. Tearney has the rights to receive royalties from this licensing arrangement. Dr. Tearney receives sponsored research funding from Canon. Dr. Tearney consults for Samsung Advanced Institute of Technology. Drs. Jaffer and Tearney receive sponsored research from Merck. Dr. Jaffer has sponsored research from Kowa Ltd.

References

1. Go AS, Mozaffarian D, Roger VL et al (2013) Heart disease and stroke statistics—2013 update: a report from the American Heart Association. Circulation 127(1):e6–e245
2. Tearney GJ, Regar E, Akasaka T et al (2012) Consensus standards for acquisition, measurement, and reporting of intravascular optical coherence tomography studies: a report from the International Working Group for intravascular optical coherence tomography standardization and validation. J Am Coll Cardiolol 59(12):1058–1072
3. Yun SH, Tearney GJ, Vakoc BJ, Shishkov M, Oh WY, Desjardins AE, Suter MJ, Chan RC, Evans JA, Jang I, Nishioka NS, de Boer JF, Bouma BE (2006) Comprehensive volumetric optical microscopy in vivo. Nat Med 12:1429–1433
4. Farooq V, Serruys PW, Heo JH, Gogas BD, Onuma Y, Perkins LE, Diletti R, Radu MD, Raber L, Bourantas CV, Zhang Y, van Remortel E, Pawar R, Rapoza RJ, Powers JC, van Beusekom HM, Garcia-Garcia HM, Virmani R (2013) Intracoronary optical coherence tomography and histology of overlapping everolimus-eluting bioresorbable vascular scaffolds in a porcine coronary artery model: the potential implications for clinical practice. J Am Coll Cardiol Intv 6(5):523–532
5. Farooq V, Gogas BD, Okamura T, Heo JH, Magro M, Gomez-Lara J, Onuma Y, Radu MD, Brugaletta S, van Bochove G, van Geuns RJ, Garcia-Garcia HM, Serruys PW (2011) Three-dimensional optical frequency domain imaging in conventional

percutaneous coronary intervention: the potential for clinical application. Eur Heart J 34(12):875–885
6. Jaffer FA, Calfon MA, Rosenthal A, Mallas G, Razansky N, Mauskampf A, Weissleder R, Libby P, Ntziachristos V (2011) Two-dimensional intravascular near-infrared fluorescence molecular imaging of inflammation in atherosclerosis and stent-induced vascular injury. J Am Coll Cardiol 57(25):2516–2525
7. Vinegoni C, Botnaru I, Aikawa E, Calfon MA, Iwamoto Y, Folco EY, Ntziachristos V, Weissleder R, Libby P, Jaffer FA (2011) Indocyanine green enables near-infrared fluorescence imaging of lipid-rich, inflamed atherosclerotic plaques. Sci Transl Med 3(84):84ra45
8. Osborn EA, Jaffer FA (2013) The advancing clinical impact of molecular imaging in CVD. JACC Cardiovasc Imaging 6(12):1327–1341
9. Jaffer FA, Verjans JW (2013) Molecular imaging of atherosclerosis: clinical state-of-the-art. Heart. doi:10.1136/heartjnl-2011-301370
10. Yoo H, Kim JW, Shishkov M, Namati E, Morse T, Shubockin R, McCarthy JR, Ntziachristos V, Bouma BE, Jaffer FA, Tearney GJ (2011) Intra-arterial catheter for simultaneous microstructural and molecular imaging in vivo. Nat Med 17:1680–1684
11. Stefanini GG, Holmes DR (2013) Drug-eluting coronary-artery stents. N Engl J Med 368:254–265
12. Camezind E, Steg P, Wijns W (2007) Stent thrombosis late after implantation of first-generation drug-eluting stents: a cause of concern. Circulation 115:1440–1455
13. Yun S, Tearney GJ, de Boer JF, Iftimia N, Bouma BE (2003) High-speed optical frequency domain imaging. Opt Express 11(22):2953–2963
14. Leitgeb R, Hitzenberger C, Fercher A (2003) Performance of fourier domain vs. time domain optical coherence tomography. Opt Express 11(8):889–894
15. Otsu N (1979) A threshold selection method from gray-level histograms. IEEE Trans Syst Man Cybern 9(1):62–66
16. Serra JP, Cressie NAC (1982) Image analysis and mathematical morphology. Academic Press, London
17. Barry JM (1973) SPLINS and SMOOTH: two FORTRAN smoothing routines. http://apo.ansto.gov.au/dspace/handle/10238/444
18. Rasband WS (1997–2014) ImageJ, U.S. National Institutes of Health, Bethesda, Maryland, USA, http://imagej.nih.gov/ij/
19. Zou KH, Warfield SK, Bharatha A, Tempany CMC, Kaus MR, Haker SJ, Wells WM, Jolesz FA, Kikinis R (2004) Statistical validation of image segmentation quality based on a Spatial Overlap Index. Acad Radiol 11(2):178–189
20. Leys C, Ley C, Klein O, Bernard P, Licata L (2013) Detecting outliers: do not use standard deviation around the mean, use absolute deviation around the median. J Exp Social Psych. http://dx.doi.org/10.1016/j.jesp.2013.03.013
21. van Soest G, Bosch JG, van der Steen AFW (2008) Azimuthal registration of image sequences affected by nonuniform rotation distortion. IEEE Trans Inf Technol Biomed 12(3):348–355
22. Ha J, Yoo H, Tearney GJ, Bouma BE (2012) Compensation of motion artifacts in intracoronary optical frequency domain imaging and optical coherence tomography. Int J Cardiovasc Imaging 28(6):1299–1304
23. Wang T, Wieser W, Springeling G, Beurskens R, Lancee CT, Pfeiffer T, van der Steen AFW, Huber RA, van Soest G (2013) Ultrahigh-speed intravascular optical coherence tomography imaging at 3200 frames per second. SPIE Proceed 8802. doi:10.1117/12.2032723
24. Schmitt JM, Bezerra H, Petroff C, Gophinat A, Trachtenberg JC (2013) Method and apparatus for automated determination of a lumen contour of a blood vessel. Software, WO/2014/092755
25. Ughi GJ, Adriaenssens T, Onsea K, Kayaert P, Dubois C, Sinnaeve P, Coosemans M, Desmet W, D'hooge J (2012) Automatic segmentation of in vivo intra-coronary optical coherence tomography images to assess stent strut apposition and coverage. Int J Cardiovasc Imaging 28(2):229–241